PRACTICAL ALTERNATIVE FOR DIFFUSING
CONSTRUCTAL NETWORK ENHANCED COLDPLATES

José L. Lage
Mechanical Engng. Dep., Southern Methodist University, Dallas-TX 75275-0337

Derli D. do Amaral Jr
Dep. of Physics, Bridgewater College, Bridgewater-VA 22812

ABSTRACT

Constructal networks for diffusion-enhanced coldplates are designed to be embedded into the solid heat generating region, which is in most cases impractical. A unique practical alternative is presented here, in which the solid conduction network is designed to be placed atop the solid cold plate, not embedded into it. This new design makes these extremely efficient and complex solid networks practical. Several networks are then designed as enhancing coldplates, following existing optimization rules, and used in realistic three-dimensional numerical simulations to determine their thermal efficiencies and to evaluate how their performances compare to the performances of the embedded design. The results indicate the alternative design yields essentially identical performance to the embedded design within the parametric range considered, making it a de-facto practical alternative for using network-enhanced cold plates.

NOMENCLATURE

D	high conductivity material height [m]
H	height [m]
i	counter
k	thermal conductivity [W/mK]
L	depth [m]
n	direction perpendicular to surface
q	heat generation rate [W]
q'''	volumetric heat generation rate [W/m^3]
T	temperature [K]
T_0	heat sink temperature [K]
T_{max}	maximum temperature [K]
V	volume [m^3]
x, y, z	Cartesian coordinates
W	width, m
Subscripts	
H	high
L	low
max	maximum

Superscript

∗   non-dimensional parameter

INTRODUCTION

Bejan[1] considered how to best distribute a finite amount of high thermal conductivity material into a rectangular, planar (i.e., one dimension being much smaller than the other two), heat-generating volume to facilitate the flow of heat out of the volume, which is adiabatic except by a small lateral isothermal area (a heat sink). This problem is equivalent to minimizing the maximum temperature attained by the heat generating volume. Originally a simple optimization challenge, the search for an appropriate solution to the high conductivity material distribution problem gives rise to an infinity of possible geometric alternatives. Following the simplest geometry for the high thermal conductivity material distribution, i.e., that of straight segments connected at 90 degrees, a set of paths resembling T-shaped networks emerge. As one proceeds from the simplest to the more complex network, the results get progressively better – meaning, the maximum temperature inside the heat generating domain gets smaller. That is, the evolution toward more complex geometries (or networks) yields an easier flow of heat out of the heat generating volume and a more efficient system. This fundamental engineering design process from simple to more complex, in turn, is observed to mimic the time evolution of several natural transport systems, systems observed to progress in time, or to evolve toward more complex geometries to achieve better, easier processes. Is this observation that gives rise to the Constructal law[2-9].

A noteworthy aspect is the high conductivity T-shaped networks obtained are supposed to be imbedded into the heat-generating volume. This distribution, called here the in-plane configuration, is disruptive and highly impractical for requiring imbedding the high conductivity material within the heat generating volume to form the networks. An alternative practical distribution is considered here, in which the very same networks of high thermal conductivity material are instead placed atop the heat generating material without directly disturbing it, in a configuration called out-of-plane. The main contribution of the present study is to ascertain how the out-of-plane configuration compares to the in-plane configuration. In doing so, practical considerations are made to design and eventually construct the cold plates, with six networks of increasing complexity being selected for comparison. Also novel, the study determines how influential to the cold plate performance is the difference between the high and low thermal conductivities of the two materials in the cold plate (i.e., the heat generating and the network).

TREE-SHAPED NETWORKS

A quick review and explanation of how the cooling networks are obtained is presented now. The fundamental volume-to-point cooling design problem proposed[1] was tackled with basic conduction principles, considering a heat generation rate q uniformly distributed within a certain planar rectangular material of thermal conductivity k_L and volume V_0, where $V_0 =$

$L_0 H_0 W$, L_0 being the depth, H_0 the height, and W the width of the volume, yielding a volumetric heat generation rate $q''' = q/(L_0 H_0 W)$. Figure 1 shows a view from the top of volume V_0. This volume is cooled via a mid-side opening of small area (heat sink), maintained at temperature T_0, centrally located at (x,y) = (0,0) in the figure, through which heat flows out, with all other boundaries being adiabatic. At steady-state, this configuration leads to a maximum temperature T_{max} in the volume, achieved at the corners (due to symmetry) opposite to the heat sink, at $x = L_o$ and $y = \pm H_o/2$.

The analysis then proceeds[1] with the utilization of a finite amount of a high thermal conductivity material, of volume V_H and conductivity k_H, to help reduce the maximum temperature in the domain. This material is to be distributed (imbedded) within the heat-generating material. Note in the analysis that both, high and low thermal conductivity materials, occupy the domain volume V_0; i.e., there is in this analysis an intrinsic assumption of the volume occupied by the high conductivity material V_H being much smaller than V_0. A first and simplest (most regular) geometric alterative for distributing the k_H material is a straight path connecting the heat sink centered at (x,y) = (0,0) to the opposite end of the volume, located at (x,y) = (0, L_o), as shown by the horizontal dashed area in figure 1. Observe the volume occupied by the high conductivity material in this simplest configuration is $V_H = L_0 D_0 W$, with D_0 being its height; hence, $V_H/V_0 = H_0/D_0$, and the requirement $V_0 \gg V_H$ translates into $D_o \ll H_o$.

The temperature difference between the heat sink temperature T_0 and the hottest spot temperature T_{max} in V_0 of Fig. 1, written as $\Delta T_0 = T_{max} - T_0$, can be shown to be equal to[1]:

$$\Delta T_o = \frac{q'''}{2k_L}\left(\frac{H_0}{2}\right)^2 + \frac{q''' H_o}{k_H D_o}\frac{L_o^2}{2} \tag{1}$$
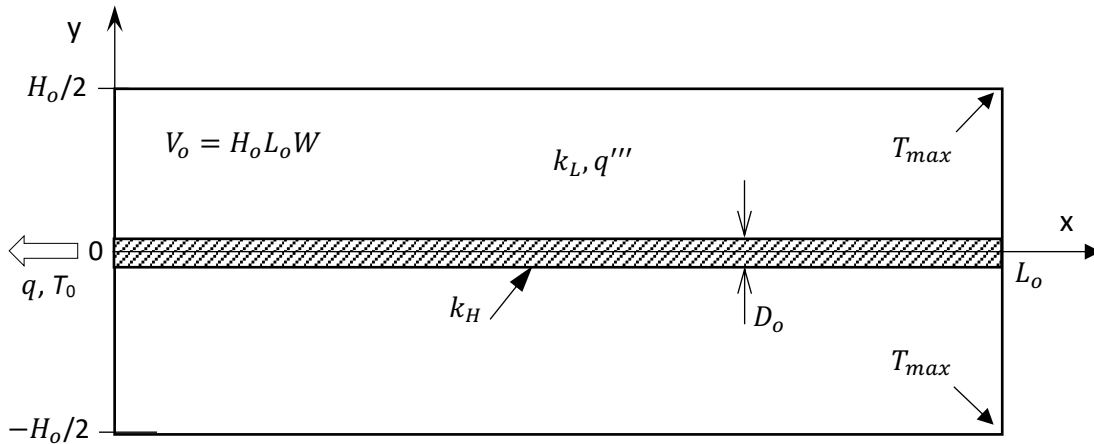

Figure 1. Elemental volume V₀ = H₀L₀W, with heat generating material k$_L$, and high thermal conductivity material k$_H$.

It is worth keeping in mind eq. (1) is an approximated result valid when the heat conduction through k_L is unidirectional in y, which is satisfied when the domain is slender, i.e., $H_o \ll L_o$. Also note eq. (1) allows for the minimization of ΔT_0 with respect to the shape of the elemental domain, H_0/L_0 (this can be seen by nondimensionalizing ΔT_0, dividing it by $q'''L_0H_0/k_L$), yielding the result:

$$\left(\frac{H_0}{L_0}\right)_{opt} = 2\left(\frac{k_L H_0}{k_H D_o}\right)^{1/2} \tag{2}$$

In view of the slenderness requirement, $H_o \ll L_o$, and remembering by construction $H_0 > D_0$, eq. (2) also requires $k_L < k_H$, which reassures the design choice of using a high thermal conductivity material, in relation to the heat generating base material. The geometrical lengths of the first assembly, $i = 0$, are now determined because H_0, D_0 and k_H, k_L are all specified by the thermal designer and eq. (2) provides $(L_0)_{opt}$, or the remaining shape relation of the first construct $i = 0$. It is important to note the optimization process leading to eq. (2) yields the length L_0 of the domain.

The evolution of the k_H distribution within k_L proceeds by realizing the need to approximate the high thermal conductivity material even more to the domain locations with maximum temperature, at the top and bottom right corners of fig. 1, to better cool the domain. This leads naturally to a second construct, $i = 1$, a T-shaped structure built by placing several optimized first constructs side-by-side perpendicular to the $y = 0$ line of the domain, as shown in figure 2 (only two $i = 0$ constructs are shown in the top right corner of the domain for visual simplicity).
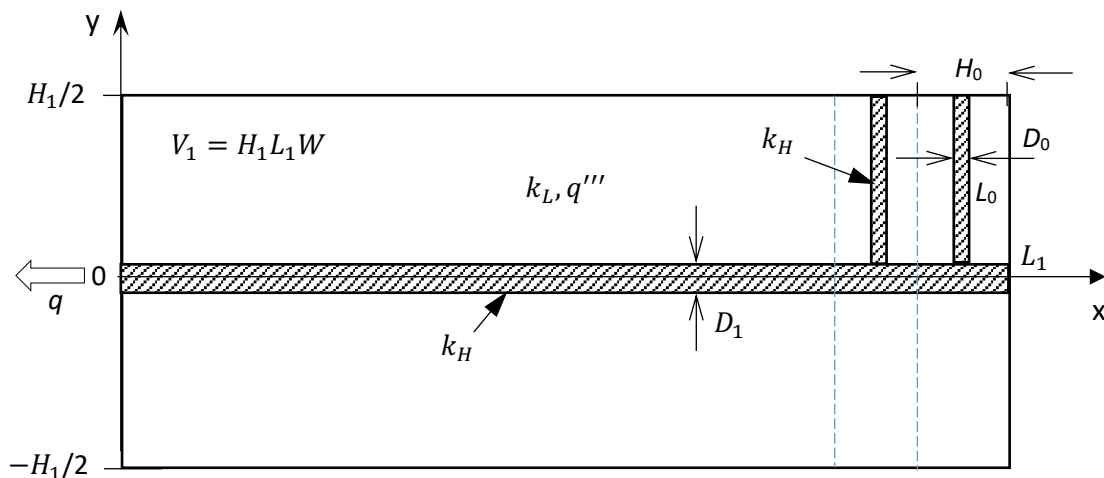

Figure 1. Volume $V_1 = H_1L_1W$, with materials k_L and k_H, showing constructs $i = 0$ (only two shown), each with H_0, D_0, L_0, and connected to k_H of construct $i = 1$ measuring L_1 and D_1.

This simple option immediately yields a geometric requirement for this second construct, namely $H_1 = 2L_{0,opt}$, which links the geometry of the first construct to the geometry of the second. The optimization of the lengths H_1, L_1 and D_1 of this second construct follows the same analysis as the optimization of the first, by reducing the visual resolution used to look at the domain to "see" the region occupied by the first construct (the regions above and below the horizontal k_H region) simply as a homogeneous heat generating region occupied by a composite material made of materials k_L and several branches of k_H.

In passing, this homogenization trick is commonly used to simplify the thermal analysis of complex porous medium systems. Under this homogenization approach, the new construct is seen exactly as the first one, as shown in figure 1, but now with a different heat generating region, still dissipating the same total amount of thermal energy but with an equivalent conductivity k_1. Observe the analysis provides the optimum number of first constructs to be connected to the horizontal (L_1,D_1) section as $n_{1opt} = 2 L_{1opt}/H_0$. Also, as n_{1opt} is expected to be an integer, the length L_{1opt} is limited by the value H_0, which is related to L_0 and D_0.

A third T-shaped construct, $i = 3$, can be imagined in a manner similar to the first and second, with additional similar steps followed by induction. Figure 3 shows the resulting structured (network) after four iterations, with the first elemental construct having length L_0, and the last having length L_4, as indicated in the figure. Only the two extreme assemblies L_0 are shown connected to L_1 in figure 3 for visual simplicity; the full network would be populated with these assemblies on both sides of L_1, filing the entire domain.
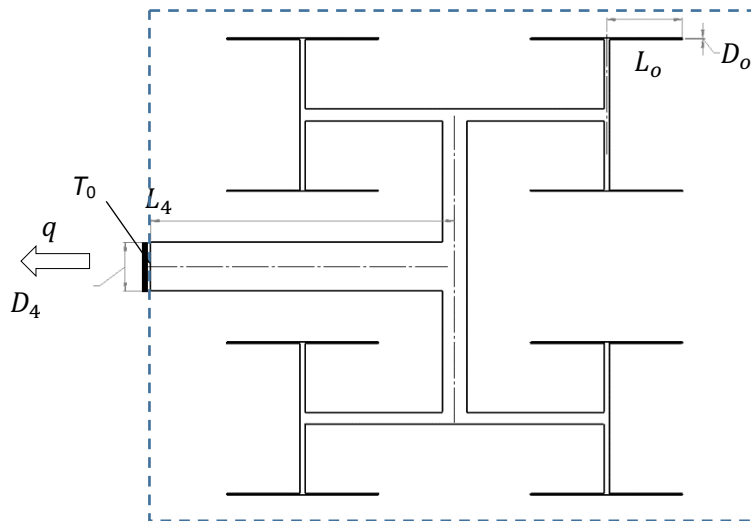

Figure 2. Assembly $i = 4$ of the T-shape network.

Also noteworthy is that, when the constructs evolve from $i = 0$, the number of branches continuously decreases; this is in line with the fact of the domain being adiabatic on the right side, making it unnecessary to fill the entire domain with high conductivity material. That is why the length of the high conductivity material of constructs larger than $i = 1$ does not cover the entire domain length; for instance, in the case $i = 4$ in figure 3, L_4 is not equal to the total depth of the domain.

Finally, every assembly construction step i is followed by the optimization of the k_H volume dimensions (i.e., assembly height H_i, depth L_i and branch height D_i; the assembly width W is kept constant for k_H being in-plane with k_L) to minimize the maximum temperature of the system. More details about the construction and the optimization process can be found elsewhere[1-9]. Table 1 shows the resulting parameters optimized for the first seven assemblies[1].

Notice the network final shape depends on the number of assemblies used, with $i = 1$, 3 and 5 yielding rectangular networks with $H_i/L_i = 2$, and $i = 2$, 4, and 6 leading to square networks with $H_i/L_i = 1$, which affects the domain shape H and L where such networks can fit. The most complex network considered here, $i = 6$ (square), has the first elemental construct having a height D_0 and depth L_0, and the last having height D_6 and depth L_6.

Table 1. Main geometric parameters of the first seven optimized assemblies[1].

Assembly i	Assembly height factor H_i/H_{i-1}	Assembly Shape[a]	Branch height factor D_i/D_{i-1}	Assembly depth factor L_i/L_{i-1}
0	-	R	-	
1	$\left(\dfrac{D_0 k_H}{H_0 k_L}\right)^{1/2} \gg 1$	R	$\left(\dfrac{D_0 k_H}{H_0 k_L}\right)^{1/2} \gg 1$	1
2	1	S	2.31	1
3	2	R	2	1
4	1	S	2	1
5	2	R	2	1
6	1	S	2	2

[a]S – square, $H_i = L_i$; R – rectangle, $L_i/H_i = 2$

PROPOSED ALTERNATIVE

It is now important to align the findings dictated by Table 1 with practice, keeping an eye on the possible manufacturability and assembly of the T-shaped cold plates. Then, hypothetically, copper and resin are seen as possibilities for the high thermal conductivity and heat generating materials, respectively, with k_H = 400 W/mK and k_L = 1.5 W/mK, due to their large difference in thermal conductivities (leading to k_H/k_L = 267), great availability, and easy machining/molding. Consider also a representative square domain with height H and depth L equal to 0.254 m (10 in) and width W equal to 6.35×10^{-3} m (¼ in). The volumetric heat generation rate dissipated in

the resin (base material, k_L) say is $q''' = 50$ kW/m^3, with a corresponding planar heat flux of about 317.5 W/m^2; the isothermal heat sink is assumed to be operating steadily at 22 °C along the side of the domain. Observe the heat sink area coincides with the area occupied by the high conductivity copper material at the left boundary of the domain (Figure 3) in all cases, while all other surfaces of the domain are considered adiabatic.

With these numbers in mind, the resin volume V_L would equal 2.561×10^{-4} m^3 (15.625 in^3) and copper $V_H = 1.536 \times 10^{-4}$ m^3 (9.375 in^3), with total cold plate volume being 4.097×10^{-4} m^3 (25 in^3). Important, for manufacturability purposes, is the smallest dimension feature of the network; here, this dimension is set to be equal or larger than 2 mm (this is the high conductivity material height D_0 of the first and smallest construct).

The height H_i, depth L_i and branch height D_i, of each assembly in each network can be now found using the data and correlations shown in Table 1. The fitting of the network within the base volume is not a simple task. The resulting geometries are generated in a CAD 3D software with a parametric link to Excel to iteratively solve for all lengths involved in each network assembly to guarantee the correct final volumes in each case. The construction of the networks is based on the smallest element of the respective assembly[9]; that is, the cold plate building process is from the smallest to the largest construct, with all dimensions having a tolerance of $\pm$ 0.2 mm (set as a convergence criterion in Excel).

Also, it is worth pointing out the resulting resin-copper volume ratio of the hypothetical cold plate, namely 1.67, does not align itself with the assumption behind Table 1, i.e., of negligible high conductivity volume. It so happens the resulting geometric relations derived from the analysis impose severe restrictions on the network geometry because the height D_0 of the smallest branch become very small very quickly when i increases. The relatively large volume of high conductivity material is the result of a tradeoff between a reasonable (manufacturable) size of the smallest branch height (limited here to 2 mm) and a reasonable (large, complex) number of branches in the network.

MODELING AND NUMERICAL SIMULATIONS

The resulting steady heat conduction process inside the cold plate is now considered within a three-dimensional domain with height H, depth L and width W, filled with two homogeneous solid materials, one (the base material) having low conductivity k_L and volumetric heat generation rate q''', and the other (the high conductivity material), forming a network, having conductivity k_H and no heat generation. Observe once a network for k_H is chosen, the parametric space affecting the thermal process within this cold plate is limited to H, D, W, k_H, k_L and q'''.

For simulating the heat transfer process in the cold plate, the balance equations valid for the regions occupied by the low and high conductivity materials are invoked, respectively:

$$\frac{\partial^2 T^*}{\partial x^{*2}} + \frac{\partial^2 T^*}{\partial y^{*2}} + \frac{\partial^2 T^*}{\partial z^{*2}} + 1 = 0 \qquad (3)$$

$$\frac{\partial^2 T^*}{\partial x^{*2}} + \frac{\partial^2 T^*}{\partial y^{*2}} + \frac{\partial^2 T^*}{\partial z^{*2}} = 0 \qquad (4)$$

where the lengths are nondimensionalized in respect to the domain depth L, i.e., $(x^*, y^*, z^*) = (x,y,z)/L$, and the nondimensional temperature is

$$T^* = \frac{T - T_0}{\frac{q'''L^2}{k_L}} \qquad (5)$$

The boundary conditions are $\partial T^*/\partial n^* = 0$, i.e., adiabatic along all external surfaces of the cold plate, with normal n, except along the heat sink where $T^* = 0$. In dealing with a heterogenous domain, compatibility conditions must be imposed along all interfaces between the base and the high conductivity materials, namely: $k^* \partial T_H^*/\partial n^* = \partial T_L^*/\partial n^*$, and $T_H^* = T_L^*$, where the new parameter $k^* = k_H/k_L$. Observe the parametric space, once a network is chosen, is now reduced to only three parameters, namely: $H^* = H/L$ and $W^* = W/L$ (note $L^* = 1$ by definition), and the thermal conductivity ratio k^*.

Equations (3) and (4), with all boundary and compatibility conditions, are solved numerically with a second-order space-accurate finite-volume scheme, with non-uniform grid distributed in all directions. The numerical grids are refined near the interfaces of the two materials to reduce the effects of heat-generation and thermal conductivity discontinuities. Extensive grid accuracy tests are performed for all network cases. All results presented here are guaranteed to be accurate to less than 1%, in terms of the difference in local temperatures within any domain, when the number of grid points used is doubled.

Because of the different resulting shape of the networks (see Table 1), two domains are considered for the simulations: one with $H^* = L^* = 1$, for the square networks i = 2, 4, and 6, and another with $H^* = 2$, $L^* = 1$, for the rectangular networks i = 1, 3, and 5. Also, the even (square) assemblies had $W^* = 0.025$ and the odd (rectangular) assemblies had $W^* = 0.0354$ - these are reasonable dimensions, considering the planar nature of the cold plates and the hypothetical considerations presented previously. Hence, the total nondimensional domain volumes are then either 0.025 for the square or 0.0708 for the rectangular domains.

All high conductivity material networks are built following Table 1, using CAD 3D with a parametric link to Excel as mentioned previously. Figure 4 shows a planar (from the top) view of the resulting six different network geometries tested. The ratio between the heat generating volume V_L and the high conductivity volume V_H is set as $V_L/V_H = 1.5$ for all cases.
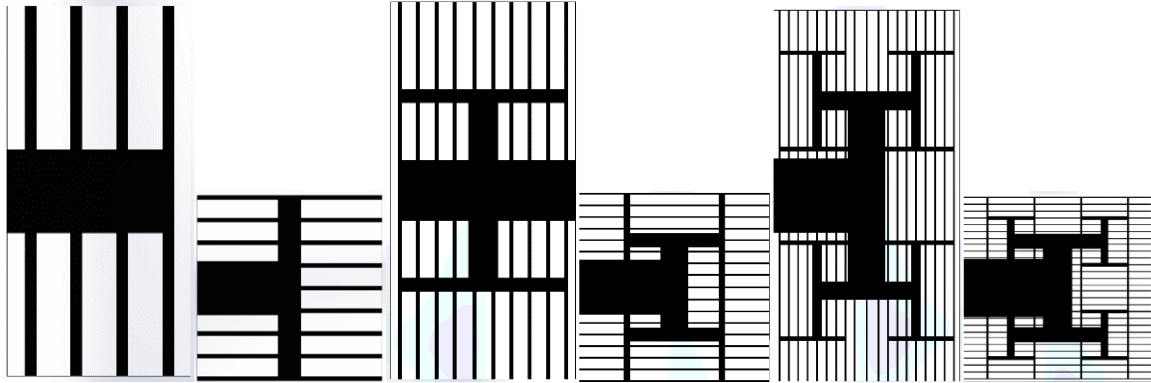
Figure 4. Resulting T-shaped networks, from left to right with i = 1 to 6.

These networks are originally conceived to be embedded into the heat generating domain. As mentioned previously, to alleviate the impractical hindrance of the original proposition, an alternative configuration considered here places the network of material k_H atop (out-of-plane) the heat generating base material k_L. In this way, the high conductivity material network need not be imbedded in the base material, but simply placed on top (or bottom) of it. Observe the width W^* of the heat generating base material in the out-of-plane configuration must be adjusted to yield the same total volume as the amount used in the in-plane configuration. Hence, W^* = 0.01562 for the square assemblies and W^* = 0.02209 for the rectangular assemblies in the out-of-plane configurations. So, for every network chosen, the in-plane and out-of-plane configurations have the same total heat generation (the same base material volumetric heat generating rate is used in all cases). The networks used in each in-plane and out-of-plane configurations are the same, so the width of material k_H in the out-of-plane network does not require any adjustment.

Figure 5 shows a side-by-side 3D renditions of the two configurations for the square network obtained with *i* = 2. Again, the thickness of the heat generating (base) material is reduced in the out-of-plane configuration, while the high conductivity material network is identical in both configurations. The size of the heat sink surface equals the size of the high conductivity material surface centered at the origin to the left of the domain, indicated with T^* = 0 in figure 5, being identical in both cases.
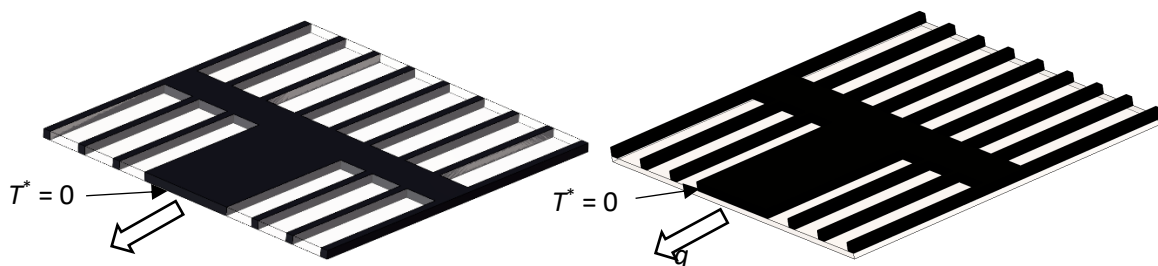

Figure 5. In-plane network (left) and out-of-plane network (right) for *i* = 2.

RESULTS

Figures 6 and 7 present, for a qualitative comparison, the T^* distribution at the top surface of the domains, side-by-side for the $i = 1$ to 6 networks (from left to right), and for the in-plane and out-of-plane configurations, respectively (out-of-plane configuration T^* distribution refers to the top of the heat generating material).

Observe the minimum temperature in the domain for all cases is $T^* = 0$ located at the heat sink surface of each cold plate (centered along the left side of the domain in the region occupied by the high conductivity material).

As seen, the results of each configuration in figures 6 and 7, are very similar to each other. Also interesting, the increase in the number of assemblies, either in the rectangular (i = 1, 3, 5) or square or rectangular (i = 2, 4, 6) shapes, makes the variation of temperature in the domain more subtle (the network branches become less discerning as i increases), as expected. This is a consequence of the easier access to the flowing heat in the domain achieved by the higher order and more complex network assemblies.
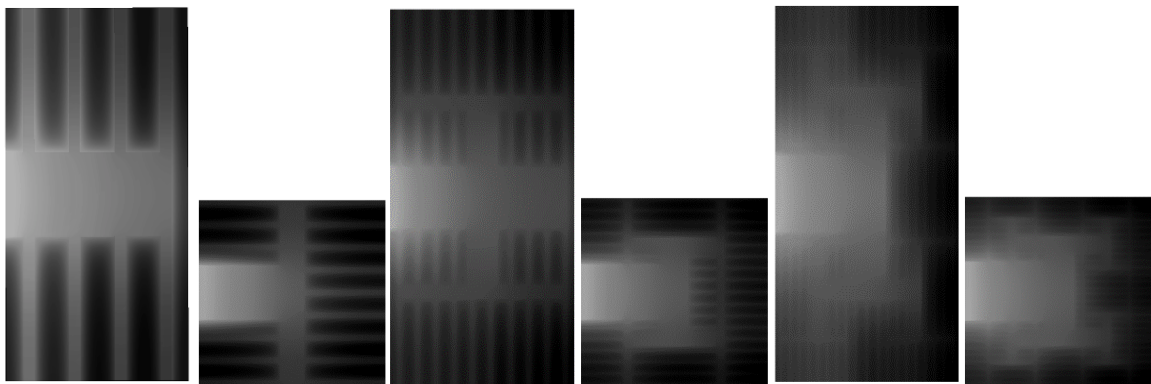

Figure 6. Temperature distribution for the in-plane (embedded) configuration, with networks i = 1 to 6 (from left to right), and k^* = 267.
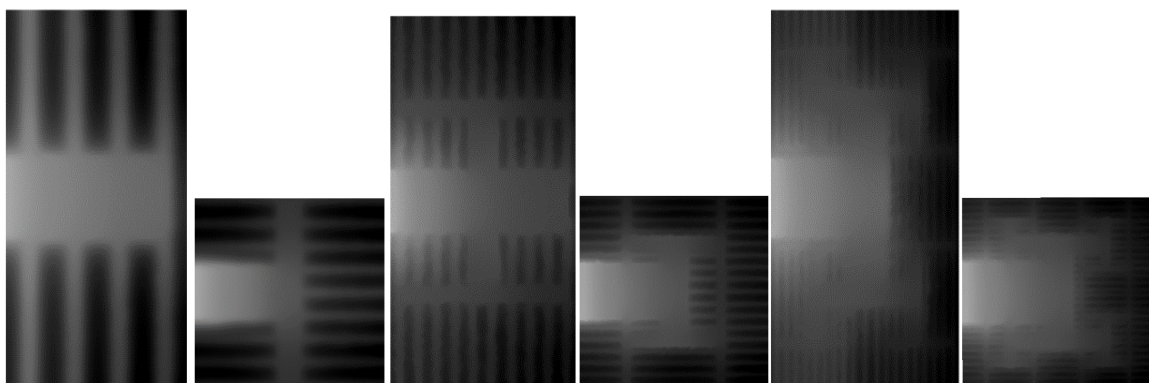

Figure 7. Temperature distribution for the out-of-plane configuration, with networks i = 1 to 6 (from left to right), and k^* = 267.

The obtained maximum temperature T^*_{max} within each domain is shown in graphical form in Figure 8, for the rectangular (i = 1, 3, 5), and for the square networks (i = 2, 4, 6). Observe the T* results are independent of the heat generation rate term q''' but not of the domain geometry, which are different when the aspect ratio of the networks differs. This explains why the temperatures of the even assemblies in Fig. 8 differ from the temperatures of the odd assemblies.
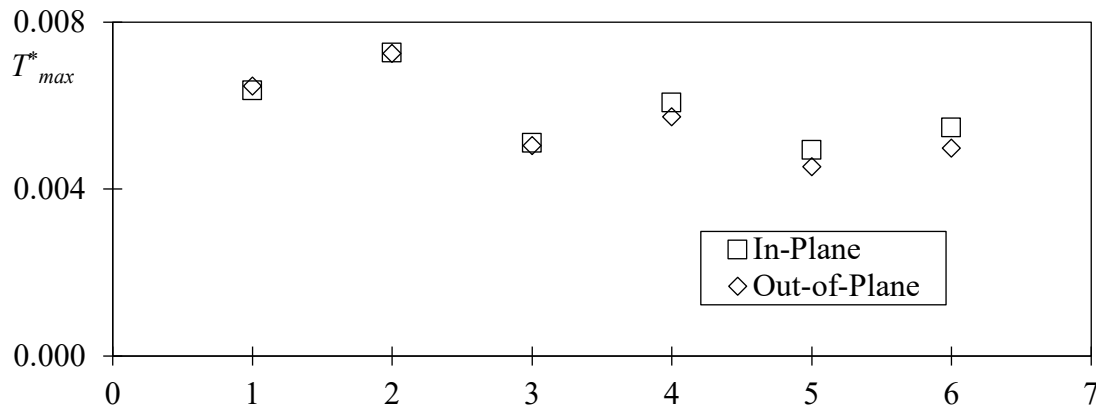

Figure 8. Maximum nondimensional temperature T*_{max} versus i for k* = 267.

The in-plane results of figure 8 fall slightly above the results for the out-of-plane configurations, with the difference becoming more pronounced with *i*. Although the difference is very small, this difference is likely a manifestation of the larger contact area between the heat generating material and the high conductivity material provided by the out-of-plane configuration in comparison to the in-plane configuration.

The graphs presented in figures 9 and 10 show T^*_{max} for similar cases as in Fig. 8, but with different k^*, from 10 to 100 in figure 9, and from 800 to 8,000 in figure 10. Figure 9, for instance, for $k^* = 10$, shows not only a large T^*_{max} value, of order 0.10, as expected when k^* is small (see Eq. (5)), but also a small variation as *i* increases. This indicates the networking role of facilitating the heat flow out of the domain is hindered when the thermal conductivities of the generating material and the high conductivity material approach each other, which makes physical sense.

Interestingly, the effect of increasing the complexity of the networks becomes very strong only when k^* increases beyond 100, figures 9 and 10. Before then the results show little change as *i* increases.

As k^* increases beyond 100, figure 10, the effect of using more complex networks (higher *i*) of high conductivity material becomes much more prevalent, particularly when *i* is smaller than 4. This aspect becomes independent of the aspect ratio of the network as well. Note, when k^* increases beyond 3,000, the effect of increasing *i* is no longer predominant. Finally, all results indicate very little difference between the in-plane and out-of-plane configurations.
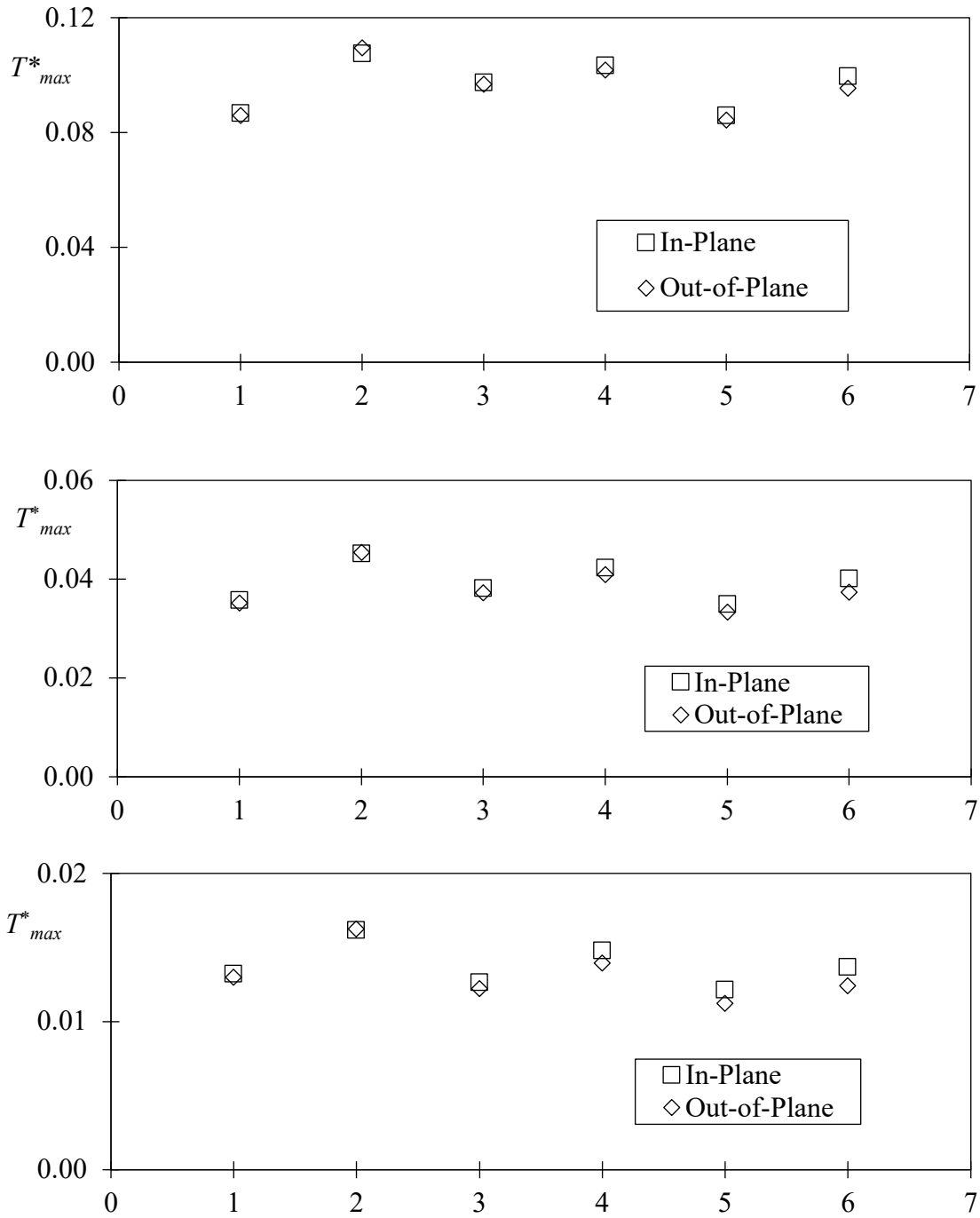
Figure 9. In-plane and out-of-plane maximum nondimensional temperature T^*_{max} versus i, for $k^* = 10$ (top), 30 (center), 100 (bottom).
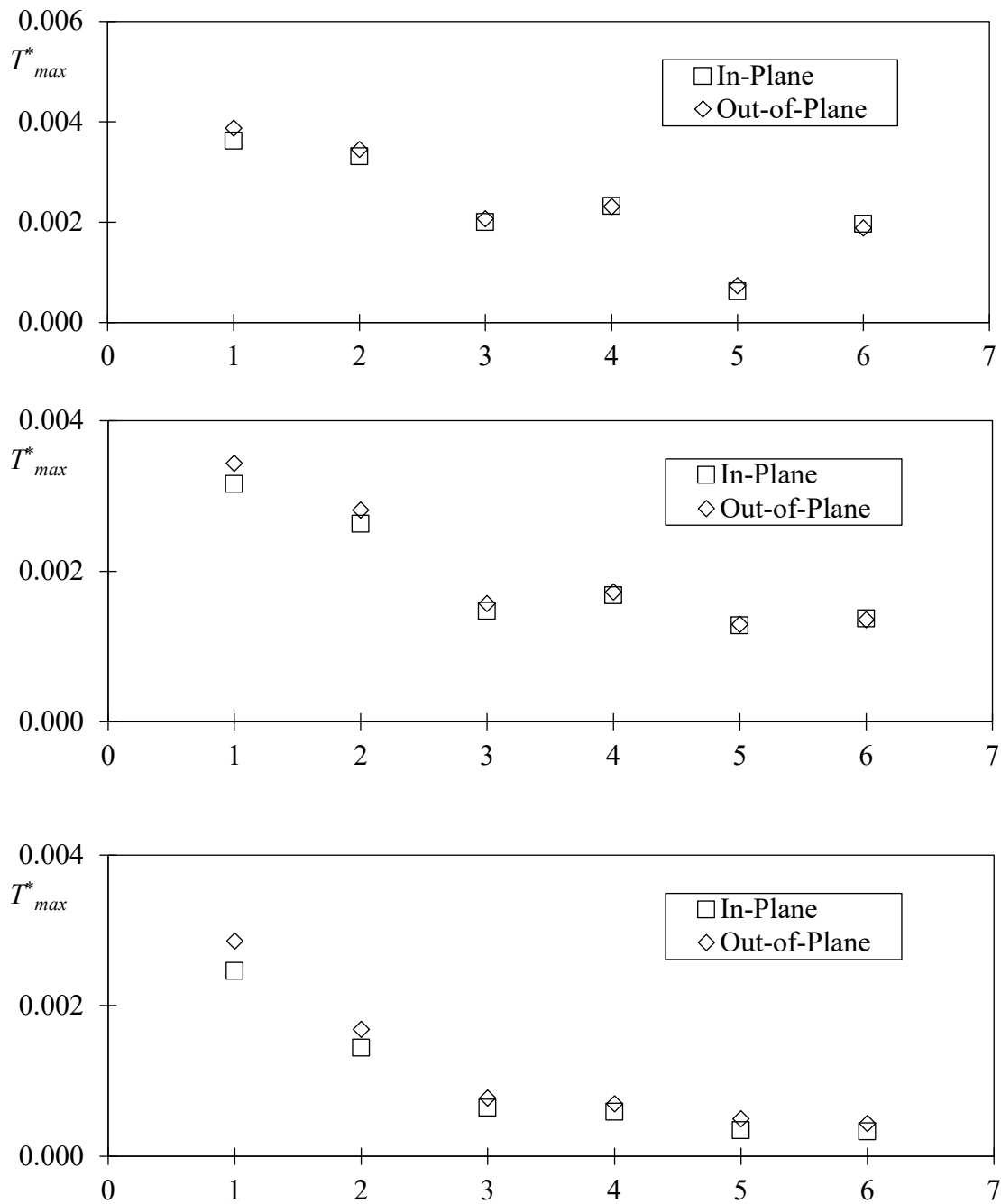
Figure 10. In-plane and out-of-plane maximum nondimensional temperature T^*_{max} versus i for k* = 800 (top), 3,000 (center), 8,000 (bottom).

A highlight of the effect of increasing k^* is shown in figure 11, where the temperature distribution of the domain is presented for k^* from 10 to 8,000, for the out-of-plane configuration with the $i = 4$ network. The effect of enhancing the flow of heat through the high conductivity material is clear as k^* increase: observe how the network becomes increasingly

more visible as k^* increases from 10 to 8,000 - the tendency is for the high conductivity material region to become more isothermal. (Note the same temperature range is used for all plots in figure 11).
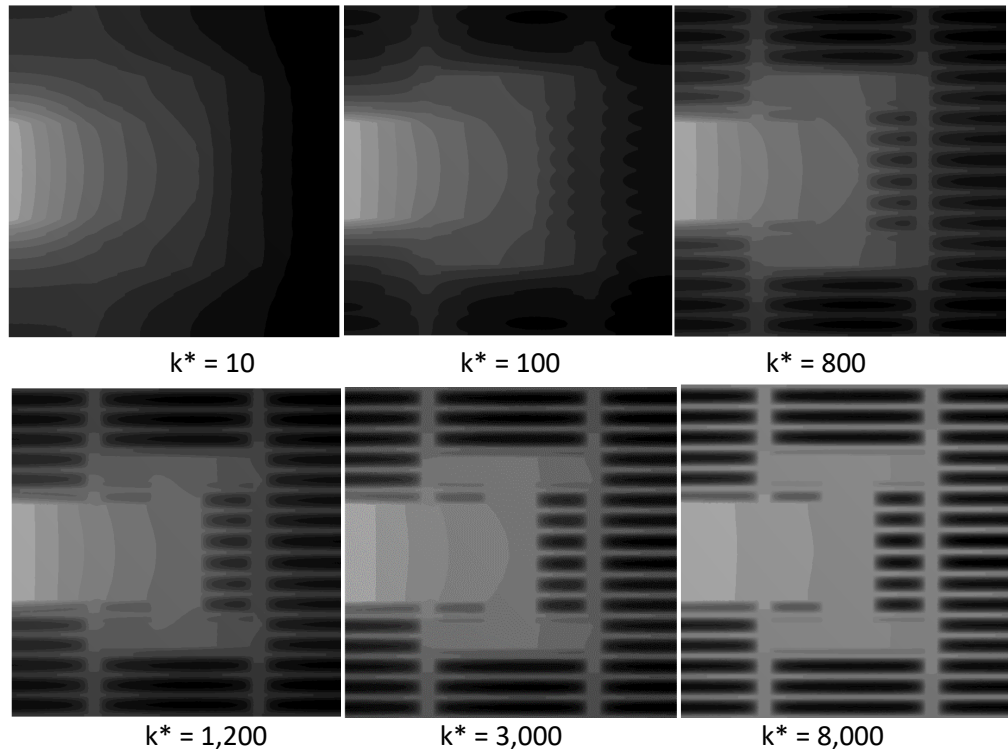

Figure 11. Effect of increasing k^* on the temperature distribution of out-of-plane with i = 4.

SUMMARY AND CONCLUSIONS

The previously proposed T-shaped networks of a high conductivity material to optimally cool a heat generating planar volume through a small side heat sink is considered from a practical point-of-view. The strong assumption of "very small" high conductivity material volume is shown to make building increasingly complex networks quickly impossible. Even when this limitation is relaxed, the other assumption of imbedding the high thermal conductivity material into the heat generating material (in-plane configuration) is also shown to be impractical in most situations. Proposed here is an alternative to circumvent this last implication by opting for an out-of-plane configuration where the networks are simply placed atop the heat generating volume. Modeling and simulation are them performed of the two resulting configurations using six increasingly complex networks, to determine how their thermal performance would compare. Also investigated is the effect, if any, of the relative thermal conductivities of heat generating and networking materials.

The numerical results indicate first the network design to be very robust: even when the original requirement of negligible high thermal conductivity material volume used is not

satisfied, the networks to cool better the heat generating material as the complexity of the design increases. This increase becomes predominant as the thermal conductivity ratio of the two materials k^* increases beyond 100, and it tends to flatten out for i larger than 3 and k^* larger than 800.

More importantly, the results show the two configurations, i.e., in-plane and out-of-plane, yield essentially identical temperature distributions. Hence, the practical utilization of the T-shaped networks becomes feasible, now that the out-of-plane configuration is shown to be as efficient as the in-plane configuration.

A final note is necessary regarding the thermal contact resistance between the surfaces of the two materials, not accounted for in the model and numerical simulations. In practice, even if the imbedded configuration is possible, the thermal contact resistance between the two materials would exist in the in-plane configuration, with the contact being restrict to the thin sides of each material. In the out-of-plane configuration, however, the contact is done along the planar surface. When i is small (0 and 1), the contact area (interface) between the two materials is then expected to be much larger in the out-of-plane configuration than in the in-plane configuration. Hence, it is possible to anticipate the present results are conservative with respect to the out-of-plane configuration, as in practice the thermal contact resistance is likely to be a more imposing hindrance to heat flow in the in-plane configuration than in the out-of-plane configuration. As the number of constructs increases ($i > 1$), the difference in contact area between the two materials is reduced, and the thermal contact effect should tend to become very similar in both cases. Again, in practice the out-of-plane configuration has the advantage of allowing for pressing the high conductivity network against the base material more easily, hence allowing for a better thermal contact, and reduced thermal resistance, than in the in-plane configuration.

ACKNOWLEDGEMENT

CONTACT

Dr. Lage is a professor of Mechanical Engineering at the Lyle School of Engineering of Southern Methodist University in Dallas, Texas. A Texas PE, he is the founder of the Thermal Transport Processes Laboratory at SMU, with research funded by the NSF, NIST, and DOE among others. He was the Associate Chair of the ME Dep, and the President of the SMU Faculty Senate. He has over 200 publications (over 5,000 citations and h = 35) and one patent. Lage is a Pi Tau Sigma

Honorary Member, an ASME Fellow, and a member of the ICHMT Scientific Council. He is the recipient of several awards, including the Sigma Xi for Outstanding Research, the ASEE for Outstanding Teaching, and the SMU Golden Mustang. He has been a Visiting Professor of the ETH-Zurich, and of the UTF-PR-Brazil and has served four years as the NSF/CBET Thermal Transport Processes program Director.

REFERENCES

1. Bejan, A. (1997). Constructal-theory network of conducting paths for cooling a heat generating volume. International Journal of Heat and Mass Transfer, 40(4), 799,813-811,816.

2. Bejan, A. (2000). Shape and structure, from engineering to nature (1. publ. ed.). Cambridge [u.a.]: Cambridge Univ. Press.

3. Reis, A. H., Miguel, A. F., & Aydin, M. (2004). Constructal theory of flow architecture of the lungs. Medical Physics, 31(5), 1135-1140.

4. Azoumah, Y., Neveu, P., & Mazet, N. (2007). Optimal design of thermochemical reactors based on constructal approach. AIChE Journal, 53(5), 1257-1266.

5. Vianna, J. C. B., Estrada, E. S. D., Isoldi, L. A., dos Santos, E. D., & Souza, J. A. (2018). A new Constructal Theory based algorithm applied to thermal problems. International journal of thermal sciences, 126, 118-124.

6. Reis, A. H., & Bejan, A. (2006). Constructal theory of global circulation and climate. International Journal of Heat and Mass Transfer, 49(11), 1857-1875.

7. Bejan, A., & Gobin, D. (2006). Constructal theory of droplet impact geometry. International Journal of Heat and Mass Transfer, 49(15), 2412-2419.

8. Morega, A. M., & Bejan, A. (2005). A constructal approach to the optimal design of photovoltaic cells. International Journal of Green Energy, 2(3), 233-242.

9. Almogbel, M., & Bejan, A. (2001). Constructal optimization of nonuniformly distributed tree-shaped flow structures for conduction. International Journal of Heat and Mass Transfer, 44(22), 4185-4194.